

## Sustainability Science and Technology



## PAPER

## OPEN ACCESS

## RECEIVED

31 December 2025

## REVISED

17 April 2026

## ACCEPTED FOR PUBLICATION

7 May 2026

## PUBLISHED

2 June 2026

Original content from this work may be used under the terms of the [Creative Commons Attribution 4.0 licence](https://creativecommons.org/licenses/by/4.0/).

Any further distribution of this work must maintain attribution to the author(s) and the title of the work, journal citation and DOI.



## Selective hydrogenolysis of glycerol to 1,3-propanediol over bifunctional Pt/KIT-6 catalysts

Joaquin Herrero<sup>1</sup> , Tobias K Misicko<sup>1</sup> , Vijaya Gopu<sup>2</sup> and Yang Xiao<sup>1,\*</sup> <sup>1</sup> Institute for Micromanufacturing and Department of Chemical Engineering, Louisiana Tech University, 505 Tech Drive, Ruston, LA 71272, United States of America<sup>2</sup> Louisiana Transportation Research Center and University of Louisiana at Lafayette, 4101 Gourrier Avenue, Baton Rouge, LA 70808, United States of America

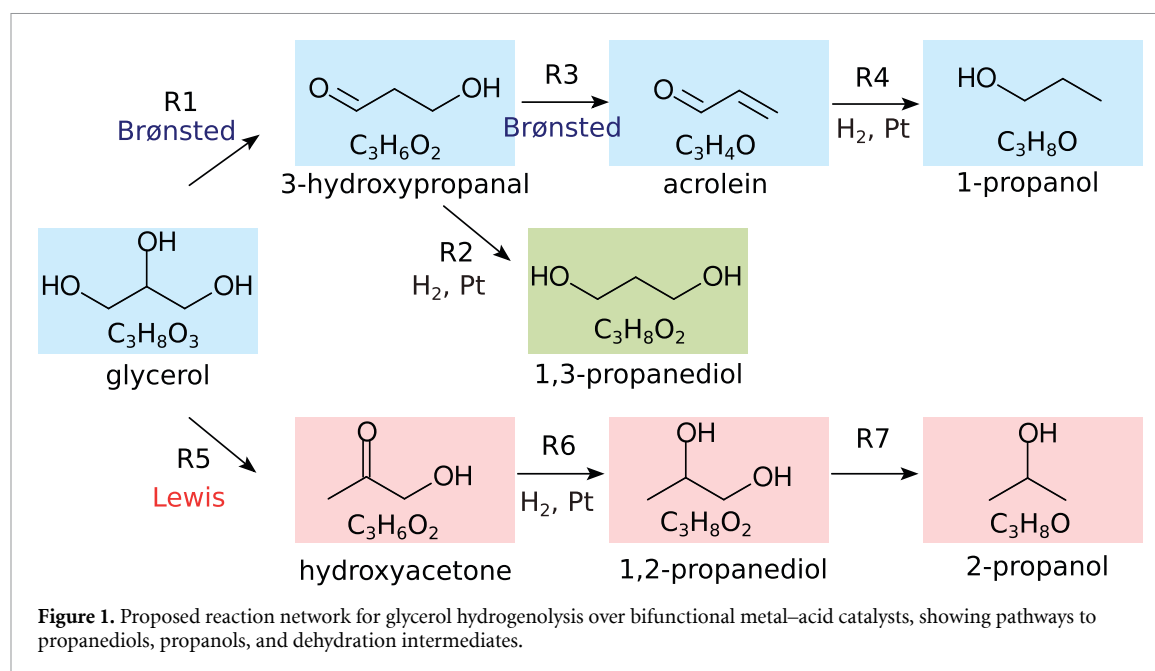
\* Author to whom any correspondence should be addressed.

E-mail: [yxiao@latech.edu](mailto:yxiao@latech.edu)**Keywords:** catalysis, reaction engineering, biodiesel, glycerol, 1,3-propanediol**Abstract**

Glycerol hydrogenolysis represents an important route for biomass valorization, enabling the sustainable conversion of glycerol, a major byproduct of biodiesel production, into value-added chemicals and thereby improving the utilization of renewable carbon resources. Selective hydrogenolysis of glycerol to 1,3-propanediol represents a critical challenge, as high selectivity requires precise control over competing C–O bond cleavage pathways on bifunctional catalysts. In this work, we establish an active-site-resolved kinetic framework to quantitatively elucidate the respective roles of metal, Brønsted acid, and Lewis acid sites in governing glycerol hydrogenolysis over Pt-based mesoporous catalysts. By systematically decoupling metal and acid site densities while preserving catalyst morphology and transport characteristics, intrinsic reaction rates and turnover frequencies for individual reaction pathways are directly quantified. Rate analysis reveals that both 1,3-propanediol formation and over-hydrogenolysis to 1-propanol are metal-mediated but are distinctly modulated by acid functionality: moderate Brønsted acidity selectively promotes 1,3-propanediol formation, whereas excessive Brønsted acidity shifts selectivity toward undesired pathways, while Lewis acid sites alone exhibit minimal promotional effects. The 0.2 wt% Pt/W–KIT-6 catalyst with a Pt site density of  $9.7 \times 10^{-6} \text{ kmol kg}_{\text{cat}}^{-1}$ , a Brønsted acid-site density of  $0.27 \times 10^{-6} \text{ kmol kg}_{\text{cat}}^{-1}$ , and a Lewis acid-site density of  $0.06 \times 10^{-6} \text{ kmol kg}_{\text{cat}}^{-1}$  exhibits approximately 12% glycerol conversion with  $\sim 80\%$  selectivity to 1,3-propanediol under 200 °C and 3 MPa H<sub>2</sub>. The Pt-site-normalized turnover frequency for the selective glycerol-to-1,3-PDO pathway is approximately  $0.07 \text{ s}^{-1}$ . Turnover frequency analysis further demonstrates that Brønsted acid sites act as true kinetic promoters rather than merely increasing apparent activity through surface coverage effects. These findings provide a mechanistically rigorous description of metal–acid cooperation in glycerol hydrogenolysis and establish a generalizable kinetic strategy for resolving active-site contributions in complex bifunctional catalytic systems, extending beyond glycerol valorization to selective hydrogenolysis and upgrading reactions involving multifunctional oxygenates.

**1. Introduction**

The rapid expansion of biodiesel and oleochemical industries has resulted in a sustained oversupply of glycerol, motivating extensive efforts toward its catalytic upgrading into value-added chemicals. Glycerol is generated in large quantities as an unavoidable by-product during the transesterification of triglycerides in biodiesel production, and its accumulation presents both economic and logistical challenges for biofuel sustainability. Consequently, catalytic routes that transform glycerol into higher-value chemicals are essential to improving the overall viability of biomass-derived fuels. Among the various transformation pathways, glycerol hydrogenolysis has attracted particular interest due to its ability to selectively cleave C–O bonds while preserving the carbon backbone, thereby enabling access to propanediols and alcohols that serve as key intermediates in polymer, pharmaceutical, and solvent industries.



However, the multifunctional nature of glycerol—containing three hydroxyl groups with distinct steric and electronic environments—renders selective C–O bond scission inherently challenging [1, 2].

Within this context, 1,3-propanediol (1,3-PDO) stands out as a particularly valuable target product [3, 4]. Compared with the more readily formed 1,2-propanediol (1,2-PDO), 1,3-PDO commands a higher market value due to its critical role in polytrimethylene terephthalate synthesis and specialty polymer applications, with global demand projected to continue increasing. From a mechanistic standpoint, the selective formation of 1,3-PDO requires the preferential activation of the secondary hydroxyl group in glycerol, a pathway that is both kinetically and thermodynamically less favorable than terminal C–O bond cleavage. As a result, achieving high selectivity and yield toward 1,3-PDO requires stringent kinetic control to suppress the competing 1,2-PDO pathway and to prevent over-hydrogenolysis to products such as 1-propanol (see figure 1). This inherent difficulty makes 1,3-PDO formation a sensitive probe of catalyst functionality and reaction control. Improving selectivity toward 1,3-propanediol is important not only from a catalytic standpoint but also from a sustainability perspective, because selective upgrading of a renewable byproduct improves feedstock utilization and reduces carbon loss to undesired reaction pathways. Figure 1 summarizes the reaction network considered in this study. Glycerol undergoes parallel and sequential transformations involving hydrogenation/dehydrogenation on Pt sites together with dehydration on Brønsted and Lewis acid sites. Selective C–O bond cleavage yields 1,3-propanediol and 1,2-propanediol (R1–R2), whereas deeper hydrogenolysis produces propanols (R3–R4). Competing dehydration routes generate intermediates such as acrolein, hydroxyacetone, and 3-hydroxypropanal (R5–R7), which may subsequently hydrogenate on Pt. This network illustrates how metal–acid cooperation governs catalytic activity and product selectivity.

Selective glycerol hydrogenolysis to 1,3-PDO is now widely recognized as a prototypical bifunctional catalytic reaction that requires the cooperative action of metallic and acidic sites [5, 6]. Metallic sites, most commonly noble metals such as Pt, Pd, and Ir, are responsible for H<sub>2</sub> activation and hydrogenation of carbonyl intermediates, while acidic sites promote dehydration and rearrangement steps that direct C–O bond cleavage. Numerous studies have demonstrated that noble metals alone preferentially produce 1,2-PDO, whereas coupling these metals with acidic oxides or acidic supports can markedly enhance selectivity toward 1,3-PDO. In particular, Brønsted acid sites facilitate the formation of key intermediates such as 3-hydroxypropionaldehyde, which are essential for the 1,3-PDO pathway, whereas Lewis acidity and excessive acidity tend to favor undesired routes and deeper hydrogenolysis.

Despite this qualitative understanding, the precise division of catalytic roles between metal and acid sites remains insufficiently resolved. It is still unclear which elementary steps are limited by metallic sites, which are promoted by Brønsted and/or Lewis acidity, and how excessive acidity redirects the reaction network toward over-hydrogenolysis [17, 18]. These uncertainties arise in part because most prior studies rely on catalyst screening approaches in which metal loading, support composition, and acidity are varied simultaneously. While such studies have successfully identified catalyst formulations capable of

**Table 1.** Representative literature studies on glycerol hydrogenolysis over bifunctional catalysts.

Catalyst	Main products	Reactor/system
Ni/WO <sub>3</sub> -ZrO <sub>2</sub> , Ni/WO <sub>3</sub> -TiO <sub>2</sub> [7]	Propanols	fixed-bed
Ni, Cu, Mg/Al <sub>2</sub> O <sub>3</sub> [8]	1,2-PDO	batch
Au-Pt/WO <sub>x</sub> /Al <sub>2</sub> O <sub>3</sub> [9]	1,3-PDO	batch
Pt/WO <sub>x</sub> /Nb <sub>2</sub> O <sub>5</sub> [10]	1,3-PDO	batch
Pt-WO <sub>x</sub> /TiO <sub>2</sub> [11]	1,3-PDO	batch
Pt/WO <sub>x</sub> /TiO <sub>2</sub> , Pt/TiO <sub>2</sub> [12]	1,3-PDO	batch
Ru-Cu/HZSM-5 [13]	1,3-PDO, 1,2-PDO	batch
NbNiAl intermetallic catalyst [14]	1,2-PDO	fixed-bed
NiAl, B-NiAl, V-NiAl [15]	1,2-PDO	batch
Cu-Ni/MgO-Al <sub>2</sub> O <sub>3</sub> [16]	1,2-PDO	batch

producing 1,3-PDO, they often obscure the kinetic origins of selectivity due to active-site ambiguity—that is, the inability to independently quantify and decouple the roles of metal sites, Brønsted acid sites, and Lewis acid sites. Consequently, reported reaction rates and selectivities are frequently interpreted phenomenologically, without clear attribution to specific active sites or rate-limiting steps. This limitation is compounded by the scarcity of active-site-normalized kinetic metrics, which prevents meaningful comparison across catalyst systems and masks transitions between metal-limited and acid-limited regimes [19–21]. As a result, the field lacks a unified kinetic framework capable of explaining why moderate Brønsted acidity enhances 1,3-PDO formation, whereas excessive acidity suppresses it and promotes over-hydrogenolysis [22].

Table 1 summarizes representative recent studies on glycerol hydrogenolysis over bifunctional catalysts. A wide range of catalytic systems has been investigated, including Pt-WO<sub>x</sub> catalysts, Au-promoted Pt catalysts, Ni- and Cu-based catalysts, as well as intermetallic NiAl materials. Although these studies demonstrate substantial progress in catalyst development and performance optimization, most investigations primarily report glycerol conversion and product selectivity without rigorous intrinsic kinetic analysis. As shown in table 1, the majority of experiments are conducted in batch reactors, while only a limited number employ continuous fixed-bed systems. Reaction rates are typically inferred from integral conversion data, and kinetic interpretations are often limited to apparent or lumped models. As a result, the individual catalytic contributions of metal sites and acid sites remain difficult to distinguish quantitatively. The absence of intrinsic, site-resolved kinetic measurements therefore continues to limit the mechanistic understanding of bifunctional catalysis in glycerol hydrogenolysis. Despite extensive studies on glycerol hydrogenolysis over bifunctional metal-acid catalysts, several important knowledge gaps remain. First, the individual catalytic roles of Pt metal sites, Brønsted acid sites, and Lewis acid sites are often intertwined, making it difficult to quantitatively resolve their respective contributions to glycerol conversion and product selectivity. Second, the mechanistic origin of the optimal metal-acid balance required for selective 1,3-propanediol formation remains insufficiently understood. Third, systematic kinetic correlations between specific acidity types and intrinsic reaction pathways are still lacking. In this work, we address these gaps through a carefully designed catalyst series with controlled acidity and by performing active-site-resolved kinetic measurements that decouple the roles of Pt metal sites, Brønsted acidity, and Lewis acidity in glycerol hydrogenolysis.

Our interest in glycerol valorization is grounded in a series of prior studies that systematically examined glycerol conversion across dehydration, oxidation, and hydrogenolysis pathways. In earlier work, we investigated glycerol dehydration and oxidation over heterogeneous catalysts, elucidating how acid type and reaction environment govern C-O bond cleavage and intermediate stability [23–25]. These studies highlighted the central role of acidity, particularly the distinction between Brønsted and Lewis acid sites, in directing reaction pathways and selectivity among competing C<sub>3</sub> products. Building on these mechanistic insights, we subsequently summarized glycerol dehydration, oxidation, and hydrogenolysis within a unified reaction-network and bond-scission framework [26], emphasizing that many glycerol transformation reactions remain limited by an incomplete understanding of metal-acid cooperation at the elementary-step level. In parallel, we have developed KIT-6-based catalyst platforms that enable independent and quantitative tuning of metal dispersion and acidity. In our prior work on Pt/KIT-6 catalysts, we demonstrated precise control over Pt surface site density and acid site properties while maintaining a well-defined mesoporous structure [27]. The present study leverages this platform to move beyond phenomenological correlations and establish active-site-resolved kinetics for glycerol hydrogenolysis. By systematically decoupling metallic and acidic functionalities, we identify the optimal balance

between Pt sites and moderate Brønsted acidity required for selective 1,3-PDO formation, providing quantitative design principles for bifunctional catalysts targeting selective C–O bond scission reactions.

## 2. Methods

### 2.1. Catalyst synthesis

Mesoporous KIT-6 silica supports were synthesized following a modified hydrothermal procedure reported in our prior work [27], yielding a three-dimensional bicontinuous cubic mesostructure with uniform mesopores and high surface area [27]. To tune the acidity of the support while preserving the KIT-6 framework, metal-incorporated KIT-6 materials (denoted as M/KIT-6, where  $M = W$  or Nb) were prepared by incorporating the corresponding metal species into the silica matrix during synthesis, following established protocols. The identity and loading of the incorporated metal were used to systematically modulate the type, density, and strength of acid sites, enabling controlled variation of Brønsted and Lewis acidity while maintaining similar textural properties across the support series. Hexachloroplatinic acid hexahydrate ( $H_2PtCl_6 \cdot H_2O$ , >99.9% metal basis, Sigma-Aldrich) was used as the Pt precursor. Platinum was introduced onto the as-synthesized supports via incipient wetness impregnation using an aqueous solution of  $H_2PtCl_6$  as the precursor. After impregnation, the samples were dried at 393 K and calcined in flowing air at 673 K for 4 h to obtain the final supported Pt catalysts. The Pt loading was systematically varied in the range of 0.1–1.0 wt% to generate a catalyst family with different surface Pt site densities. Importantly, when Pt loading was varied on a given M/KIT-6 support, the intrinsic acidity of the support remained essentially unchanged, allowing independent control of metallic site density and acid site density. This synthesis strategy produced a well-defined catalyst platform in which Pt surface sites, Brønsted acid sites, and Lewis acid sites could be independently tuned. Such independent control is essential for decoupling metal-mediated and acid-mediated reaction steps and for enabling active-site-resolved kinetic analysis of glycerol hydrogenolysis. Prior to catalytic testing, all catalysts were sieved to a particle size of 250–355  $\mu m$  to minimize intraparticle diffusion limitations and ensure consistent hydrodynamic conditions across experiments.

### 2.2. Catalyst characterization

Textural properties of all KIT-6-based supports and Pt-loaded catalysts were determined by  $N_2$  physisorption at 77 K using a Micromeritics ASAP 2020 instrument [27]. Prior to measurements, samples were degassed under vacuum to remove adsorbed moisture and volatiles. Specific surface areas were calculated using the Brunauer–Emmett–Teller method, and pore size distributions were obtained from the adsorption/desorption isotherms using the Barrett–Joyner–Halenda (BJH) model. Powder x-ray diffraction was used to confirm preservation of the ordered mesostructured framework after metal incorporation, Pt loading, and post-treatment. Platinum dispersion and particle size distributions were evaluated by a combination of chemisorption and transmission electron microscopy (TEM). In line with our prior work on mesoporous Pt-supported catalysts, Pt dispersion was quantified by chemisorption-based titration methods and converted to the number of exposed surface Pt sites [27]. Representative TEM images were acquired using an FEI Tecnai instrument operated at 200 KV (LaB<sub>6</sub> source), and particle size distributions were obtained by measuring a statistically meaningful number of particles across multiple micrographs [27]. For rate normalization, the number of exposed Pt surface sites was used to compute intrinsic turnover frequencies, with the adsorption stoichiometry defined consistently for the chemisorption protocol employed. A 0.5% Pt/Al<sub>2</sub>O<sub>3</sub> standard catalyst (metal dispersion =  $31 \pm 0.5\%$ , Micromeritics) was used as the calibration reference for H<sub>2</sub> chemisorption and H<sub>2</sub>–O<sub>2</sub> titration measurements. Acidic properties were quantified using both NH<sub>3</sub> temperature-programmed desorption (NH<sub>3</sub>-TPD) and pyridine-adsorbed infrared spectroscopy. NH<sub>3</sub>-TPD experiments were performed using a Micromeritics AutoChem II 2920 analyzer coupled with a mass selective detector to identify evolved gaseous species [27]. Catalyst samples were packed between quartz wool plugs in a U-shaped quartz cell, purged in ultra-high-purity He (50 std ml min<sup>-1</sup>) to remove physisorbed species, and then subjected to programmed heating to high temperature to obtain desorption profiles and total acid site densities. The NH<sub>3</sub>-TPD results were used as an independent measure of total acidity. To differentiate Brønsted and Lewis acid site densities, diffuse-reflectance FTIR/DRIFTS spectra of adsorbed pyridine were collected using a Tensor-27 spectrometer equipped with a Pike diffuse reflectance accessory [27]. In a typical measurement, ~25 mg of catalyst was pretreated (oxidative pretreatment), exposed to pyridine, and then heated to desorb pyridine under a controlled temperature ramp. Prior to IR acquisition, physisorbed pyridine was removed by evacuation at moderate temperature (e.g., 120 °C), and spectra were recorded at multiple temperatures to confirm the robustness of quantified acid site densities. Brønsted- and

Lewis-bound pyridine were assigned to bands near 1550 and 1455  $\text{cm}^{-1}$ , respectively, and acid site densities were calculated from integrated band areas using established extinction coefficients. Since reaction selectivity is highly sensitive to working-condition acidity, pyridine-IR quantification was performed at temperatures relevant to catalytic testing, consistent with our prior methodology [27]. The quantified densities of surface Pt sites, Brønsted acid sites, and Lewis acid sites were used to normalize reaction rates and compute intrinsic turnover frequencies (TOFs) for the competing hydrogenolysis pathways. This site-resolved framework enables direct identification of kinetically relevant active sites and disentangles metal-mediated hydrogenation steps from acid-catalyzed dehydration/rearrangement and C–O bond scission pathways.

### 2.3. Catalytic performance evaluation

Catalytic performance for glycerol hydrogenolysis was evaluated in a batch reactor system. All reactions were carried out in a stirred Parr high-pressure reactor, following procedures established in our prior glycerol conversion studies [24]. In a typical experiment, a known amount of catalyst and aqueous glycerol solution were charged into the reactor, which was then purged and pressurized with hydrogen to the desired pressure. The reactor was heated to the target temperature under continuous stirring, and the reaction was allowed to proceed for a specified reaction time. After completion, the reactor was quenched, depressurized, and the liquid products were collected for analysis. Because the experiments were conducted in batch mode, catalytic activity and selectivity are reported as functions of reaction time rather than time-on-stream. To ensure that the measured reaction rates reflect intrinsic catalytic kinetics, the absence of heat- and mass-transfer limitations was carefully assessed. The evaluation followed the same rigorous methodology developed and validated in our previous kinetic studies of glycerol conversion [25]. External mass-transfer limitations were minimized by vigorous stirring and confirmed by verifying that further increases in stirring rate did not affect glycerol conversion or product selectivity. Internal diffusion limitations were mitigated by using finely sieved catalyst particles and were further evaluated using standard diagnostic criteria. Specifically, the Weisz–Prater criterion for internal mass-transfer resistance was satisfied under all reaction conditions, indicating that intraparticle diffusion did not influence the observed reaction rates [28, 29]. In addition, the Mears criterion for external mass-transfer limitations and the Mears criterion for heat-transfer limitations were both satisfied, confirming the absence of significant concentration or temperature gradients between the bulk liquid phase and the catalyst surface. These analyses demonstrate that the catalytic performance data reported in this study are free from transport artifacts and can be directly interpreted in terms of intrinsic reaction kinetics and active-site effects. Intrinsic kinetic measurements were conducted under conditions designed to ensure reliable initial-rate analysis in the batch reactor system. Hydrogen was supplied at sufficiently high initial pressure to maintain  $\text{H}_2$  in large excess relative to glycerol during the time window used for rate determination. The dissolved hydrogen concentration was estimated using Henry's law, and no measurable pressure decrease was observed during the reaction period analyzed. Liquid–solid mass-transfer limitations were evaluated by performing experiments at different stirring speeds; the reaction rate was independent of stirring speed above 800 rpm, indicating negligible external diffusion resistance. In addition, the catalyst particle size was smaller than 100 mesh, which minimizes potential internal diffusion limitations. All intrinsic kinetic parameters were derived from initial-rate measurements obtained at low glycerol conversion (<10%). Under these conditions, concentration gradients and product inhibition effects are negligible, and the system approximates differential operation, allowing reliable extraction of intrinsic catalytic reaction rates.

Compositions of glycerol and reaction products were quantitatively analyzed using a gas chromatograph (Agilent GC 6890) equipped with a flame ionization detector and an UltiMetal capillary column (15 m  $\times$  0.32 mm  $\times$  0.10  $\mu\text{m}$ ) with a retention gap. High-purity gases including  $\text{O}_2$  (99.98%), Ar (99.999%),  $\text{N}_2$  (99.999%), He (99.98%), and  $\text{H}_2$  (99.999%) were used. Control experiments were conducted to clarify the role of each catalyst component. The unsupported W-KIT-6 catalyst (without Pt, see figure 5(a)) exhibited negligible glycerol conversion (<0.5%) under the studied conditions. Additional blank tests using Pt/ $\text{SiO}_2$  and pure  $\text{SiO}_2$  KIT-6 were also performed and similarly showed negligible conversion (<0.5%). These results indicate that neither the silica support nor isolated metal sites alone produce measurable activity, confirming that the observed glycerol hydrogenolysis requires the combined metal-acid functionality of the Pt/M-KIT-6 catalysts.

### 2.4. Definitions of conversion, selectivity, reaction rate, and turnover frequency

Glycerol conversion ( $X_{\text{GLY}}$ ) was defined as the fraction of glycerol consumed relative to the initial amount charged to the batch reactor, calculated on a molar basis:

$$X_{\text{GLY}} = \frac{n_{\text{GLY}}(0) - n_{\text{GLY}}(t)}{n_{\text{GLY}}(0)}$$

where  $n_{\text{GLY}}(0)$  and  $n_{\text{GLY}}(t)$  denote the initial and time-dependent moles of glycerol, respectively.

Product selectivity toward species  $i$  ( $S_i$ ) was defined on a carbon-molar basis as:

$$S_i = \frac{\nu_i n_i}{\sum_j \nu_j n_j}, \quad (1)$$

where  $n_i$  is the number of moles of product  $i$ ,  $\nu_i$  is the number of carbon atoms in species  $i$ , and the summation includes all quantified carbon-containing products. Product yield ( $Y_i$ ) was defined as the product of conversion and selectivity:

$$Y_i = X_{\text{GLY}} \times S_i. \quad (2)$$

Initial reaction rates were determined from the slope of the molar amount of reactant consumed or product formed as a function of reaction time in the initial linear regime (typically  $X_{\text{GLY}} < 10\%$ ), where concentration changes and secondary reactions are minimal. For product  $i$ , the rate was calculated as:

$$r_i = \frac{1}{m_{\text{cat}}} \left( \frac{dn_i}{dt} \right)_{t \rightarrow 0}, \quad (3)$$

where  $m_{\text{cat}}$  is the mass of catalyst used. Rates are thus expressed in units of  $\text{mol g}_{\text{cat}}^{-1} \text{s}^{-1}$ .

TOFs were obtained by normalizing the intrinsic reaction rates by the number of catalytically relevant active sites. For a given reaction pathway  $k$  controlled by site type  $m$  (Pt, Brønsted acid, or Lewis acid), the TOF was defined as:

$$\text{TOF}_{k,m} = \frac{r_k}{N_m}, \quad (4)$$

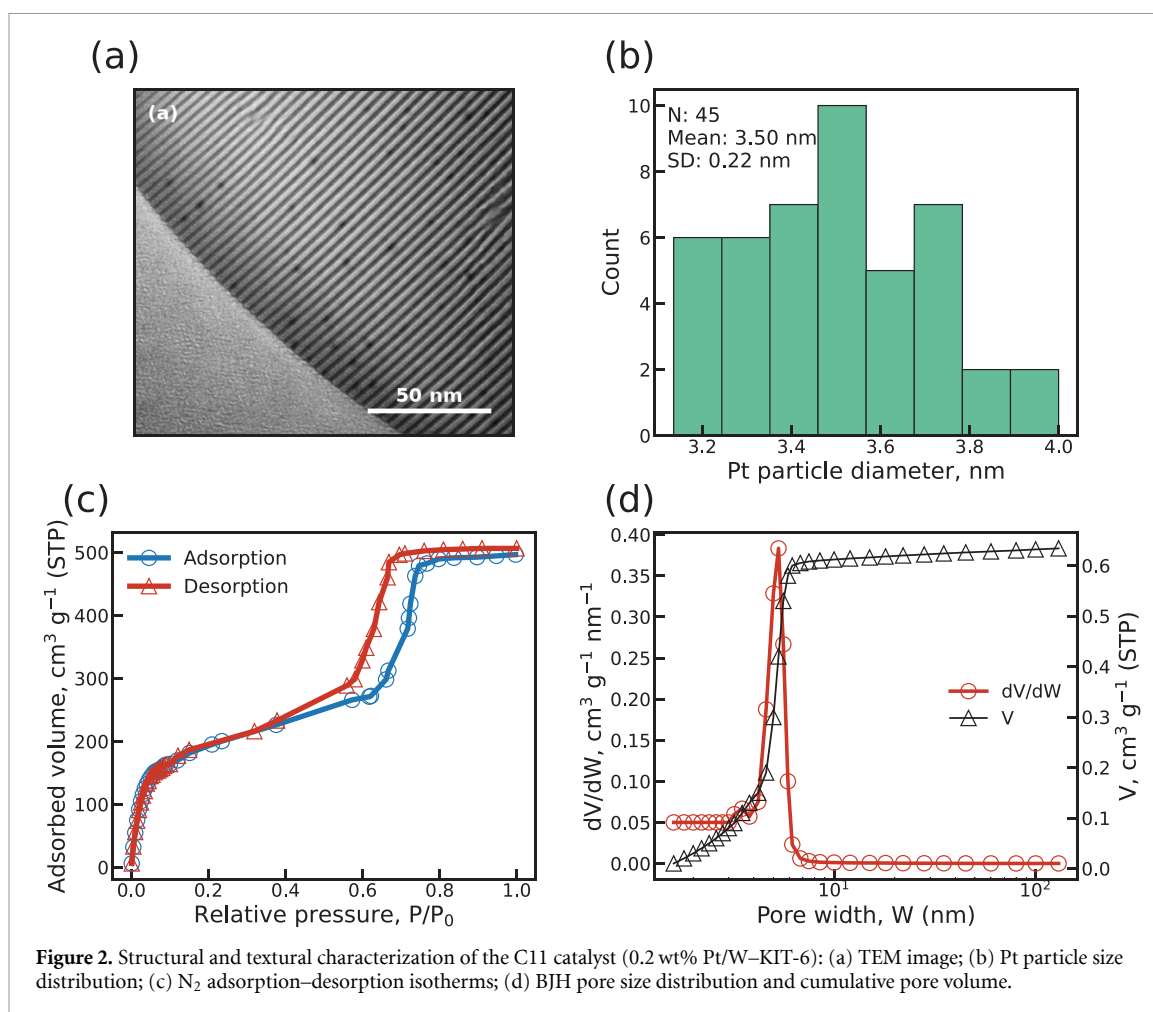
where  $r_k$  is the initial rate associated with pathway  $k$ , and  $N_m$  is the total number of active sites of type  $m$ , as quantified by chemisorption or acid-site titration methods.

### 3. Results and discussion

For clarity, catalysts are identified using the same sample labels (e.g. C06, C11, C15) established in our prior work [27]. Each label uniquely corresponds to a specific combination of support composition, Pt loading, and calcination conditions, and is used consistently throughout this study. Although the numerical identifiers are not sequential, they reflect the historical synthesis order and provide continuity with previous publications. To facilitate mechanistic interpretation, the catalysts are organized into three sets (A–C), each designed to systematically isolate the effects of Pt site density, Brønsted acid site density, or Lewis acid site density, respectively, while holding other properties approximately constant (tables 2–4).

#### 3.1. Structural characterization of Pt/KIT-6 catalysts

The structural and textural properties of the C11 catalyst (0.2 wt% Pt/W–KIT-6), which serves as the representative catalyst in the performance evaluation, were systematically characterized using electron microscopy and  $\text{N}_2$  physisorption measurements, as summarized in figure 2. Representative TEM images (figure 2(a)) reveal a high degree of Pt nanoparticle dispersion on the three-dimensionally ordered mesoporous KIT-6 support, with no evidence of large agglomerates or support structural collapse. The interconnected bicontinuous pore network of KIT-6 remains intact after Pt deposition, indicating that the impregnation and reduction procedures do not disrupt the mesostructure. Quantitative analysis of the TEM images yields the Pt particle size distribution shown in figure 2(b). The Pt nanoparticles exhibit a narrow size distribution centered in the 3–4 nm range, with a limited population of particles outside this interval. The relatively small standard deviation indicates uniform nucleation and growth of Pt particles within and on the surface of the KIT-6 mesopores. Such uniform Pt dispersion is essential for isolating intrinsic structure–activity relationships by minimizing variations in exposed metal surface area across catalyst samples. The textural properties of the C11 catalyst were further examined by  $\text{N}_2$  adsorption–desorption measurements at 77 K (figure 2(c)). The isotherms display a characteristic type IV profile with a pronounced H1-type hysteresis loop, consistent with a well-defined mesoporous structure and a narrow pore size distribution. The steep capillary condensation step at intermediate relative pressures reflects the uniform mesopores of KIT-6, while the absence of low-pressure micropore filling suggests that microporosity is negligible. Importantly, the overall shape of the isotherm and the presence of



the hysteresis loop confirm that the ordered mesoporous framework of KIT-6 is preserved following Pt incorporation. Pore size distribution analysis derived from the desorption branch using the BJH method is shown in figure 2(d). The BJH pore size distribution shows a dominant mesopore population centered at approximately 8.5–10 nm, consistent with the characteristic mesoporous structure of KIT-6. A weak distribution tail extending to larger pore widths (up to ~120 nm) is also observed, but this corresponds only to a minor fraction of wider pores rather than the dominant pore population. The cumulative pore volume profile further confirms the preservation of the mesoporous framework. The various catalysts exhibit similar surface areas (720–810 m<sup>2</sup> g<sup>-1</sup>), average pore sizes (8.5–10 nm), and pore volumes (0.8–1.1 cm<sup>3</sup> g<sup>-1</sup>) at the targeted Pt loading, indicating that metal incorporation does not significantly alter the mesostructure of the KIT-6 support. The preservation of mesopore accessibility is critical for facilitating molecular transport and ensuring that the observed catalytic trends arise from intrinsic active-site effects rather than diffusion limitations. Mesoporous silica KIT-6 was selected as the catalyst support due to its three-dimensional mesoporous pore structure and high surface area. These structural features promote uniform dispersion of Pt nanoparticles and facilitate diffusion of bulky polyol molecules such as glycerol. Compared with conventional supports such as SBA-15,  $\gamma$ -Al<sub>2</sub>O<sub>3</sub>, or amorphous silica, the three-dimensional pore connectivity of KIT-6 reduces diffusion limitations, which is advantageous for intrinsic kinetic investigations. Furthermore, the chemically inert silica framework provides a neutral platform for the controlled introduction of Brønsted and Lewis acid functionalities, enabling independent tuning of metal and acid sites required for active-site-resolved kinetic analysis.

### 3.2. Results of measured acidity

Figure 3 summarizes the acidity characteristics of Pt/Nb-KIT-6 catalysts calcined at 550 °C (C21, 1.0 wt% Pt/Nb-KIT-6) and 650 °C (C22, 1.0 wt% Pt/Nb-KIT-6), as quantified by complementary NH<sub>3</sub>-TPD and pyridine-adsorbed FTIR spectroscopy. These two techniques provide, respectively, the total acid site density and the distribution of Brønsted and Lewis acid sites, enabling a rigorous and internally consistent assessment of catalyst acidity. Figure 3(a) shows the NH<sub>3</sub>-TPD profiles of C21 and C22. Both

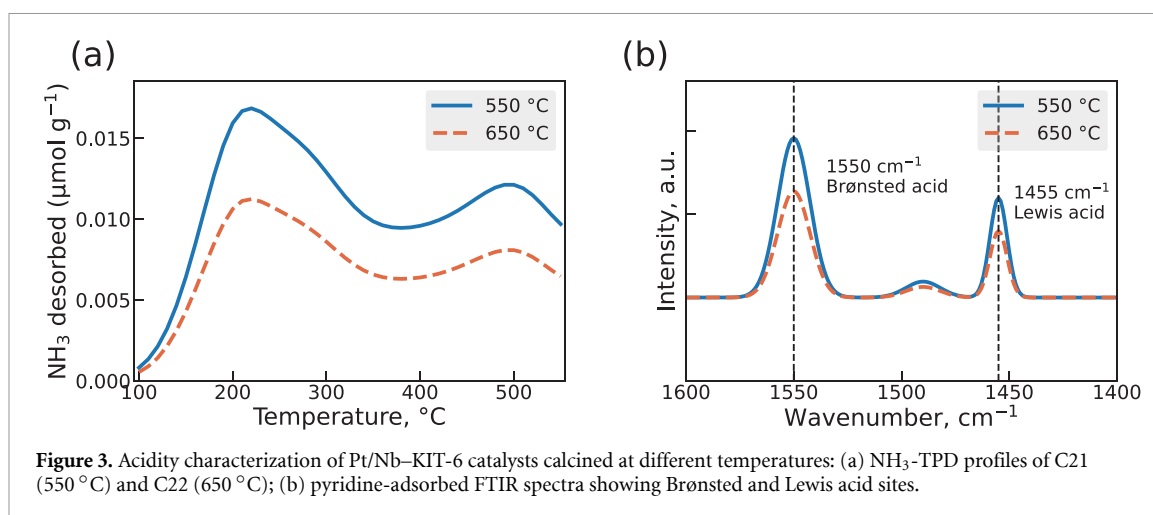


**Figure 3.** Acidity characterization of Pt/Nb-KIT-6 catalysts calcined at different temperatures: (a)  $\text{NH}_3$ -TPD profiles of C21 (550 °C) and C22 (650 °C); (b) pyridine-adsorbed FTIR spectra showing Brønsted and Lewis acid sites.

catalysts exhibit a broad desorption feature spanning approximately 150 °C–400 °C, indicative of predominantly weak-to-moderate acid sites, with no pronounced sharp peak at very high temperatures. This behavior suggests the absence of a significant population of strong acid sites, which are often associated with excessive dehydration and coke formation in polyol hydrogenolysis reactions. The overall desorption intensity of C21 is systematically higher than that of C22 across the entire temperature range, reflecting a higher total acid site density for the catalyst calcined at the lower temperature. Integration of the  $\text{NH}_3$ -TPD profiles yields total acidities of  $0.24 \mu\text{mol g}^{-1}$  for C21 and  $0.16 \mu\text{mol g}^{-1}$  for C22, consistent with values independently obtained from pyridine-based measurements. The reduction in total acidity upon calcination at 650 °C is attributed to partial dehydroxylation and structural condensation of Nb–O–Si species, which decreases the density of accessible acid sites. Figure 3(b) presents the pyridine-adsorbed FTIR spectra of C21 and C22 collected in the 1600–1400  $\text{cm}^{-1}$  region. Two well-defined bands are observed for both catalysts: a band centered at  $\sim 1550 \text{ cm}^{-1}$ , corresponding to pyridinium ions formed on Brønsted acid sites, and a band at  $\sim 1455 \text{ cm}^{-1}$ , associated with coordinatively bound pyridine on Lewis acid sites. The presence of both bands confirms the bifunctional acidic nature of Nb-incorporated KIT-6 supports. Comparison of the spectra indicates that the intensities of both Brønsted and Lewis acid bands decrease from C21 to C22, in agreement with the lower total acidity measured by  $\text{NH}_3$ -TPD. Importantly, the relative intensity ratio of the Brønsted to Lewis acid bands remains approximately constant at  $\sim 3:1$  for both catalysts, indicating that calcination primarily reduces the absolute number of acid sites without significantly altering the Brønsted/Lewis acid balance. The  $\text{NH}_3$ -TPD and pyridine-adsorbed FTIR results demonstrate that Pt/Nb-KIT-6 catalysts possess a well-defined population of predominantly moderate-strength acid sites with Brønsted-dominated acidity. Calcination at higher temperature decreases the total acid site density while preserving the Brønsted/Lewis acid ratio. This controlled tuning of acidity provides a well-defined basis for correlating acid site density and type with catalytic activity and selectivity in glycerol hydrogenolysis, as discussed in the following kinetic analysis. The W and Nb species are incorporated into the KIT-6 framework to introduce controlled acidic functionalities within the mesoporous support. These heteroatoms generate Brønsted and/or Lewis acid sites that facilitate glycerol dehydration steps required for the formation of intermediates leading to 1,3-propanediol. In the bifunctional catalytic mechanism, dehydration occurs on acid sites while hydrogenation occurs on adjacent Pt sites. Therefore, the primary role of W/Nb is to tune the type, density, and strength of acid sites involved in the dehydration step. In addition, incorporation of W or Nb may influence metal-support interactions and slightly modify the dispersion or electronic environment of Pt, which can indirectly affect hydrogenation kinetics.

### 3.3. Results of catalytic performance

Figure 4 summarizes the catalytic performance of the C11 catalyst (0.2 wt% Pt/W-KIT-6) for glycerol hydrogenolysis, elucidating the effects of reaction time, temperature, and hydrogen pressure on glycerol conversion, product selectivity, and 1,3-propanediol (1,3-PDO) yield. The observed product distributions are interpreted in the context of the glycerol reaction network shown in figure 1, where selective C–O hydrogenolysis routes compete with consecutive over-hydrogenolysis pathways. Under standard reaction conditions (200 °C, 3 MPa  $\text{H}_2$ , 1.0 g catalyst) in figure 4(a), glycerol conversion increases rapidly at early reaction times and gradually approaches a quasi-steady value of approximately 12% after about 5 h. In

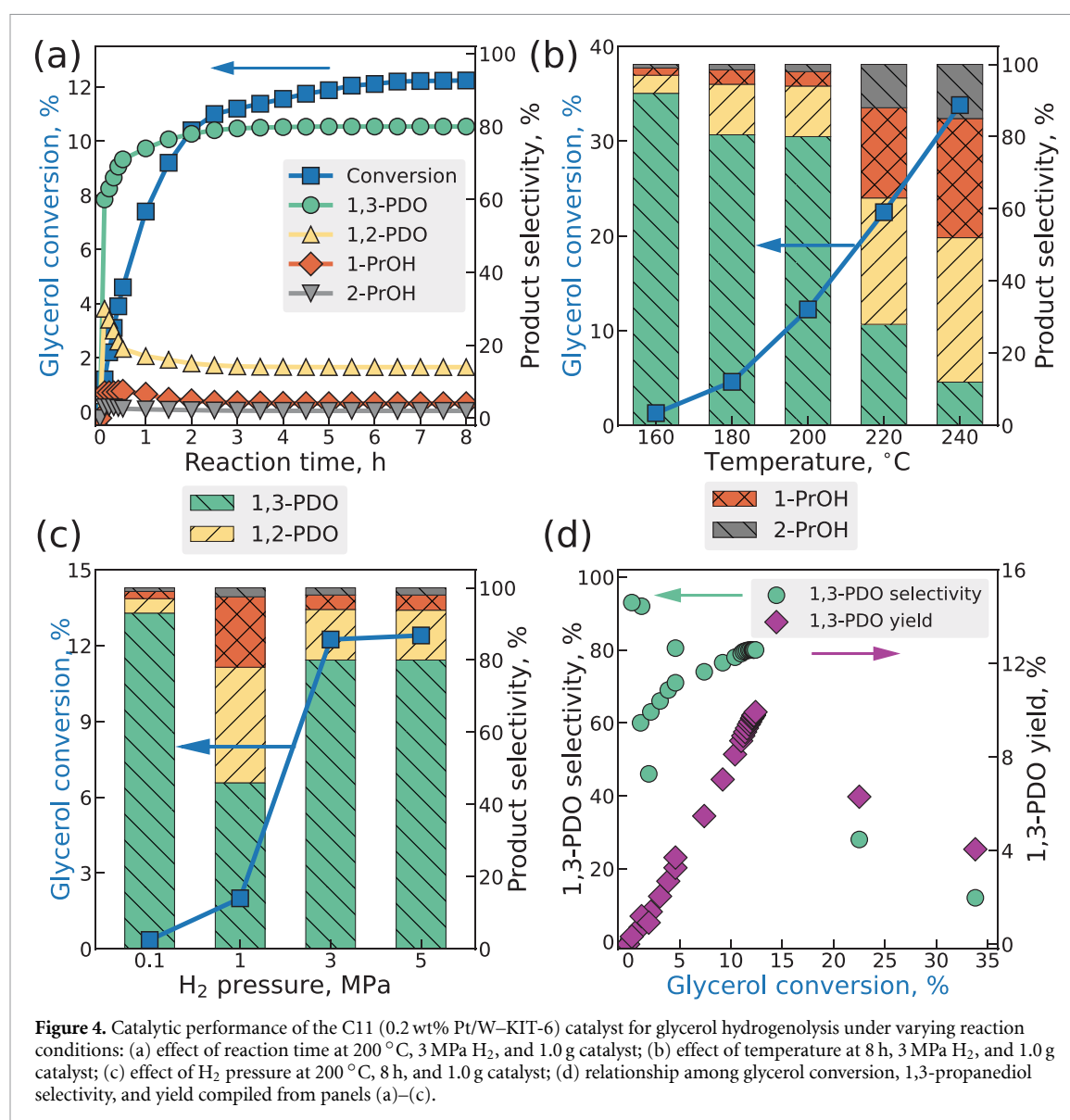


**Figure 4.** Catalytic performance of the C11 (0.2 wt% Pt/W–KIT-6) catalyst for glycerol hydrogenolysis under varying reaction conditions: (a) effect of reaction time at 200 °C, 3 MPa H<sub>2</sub>, and 1.0 g catalyst; (b) effect of temperature at 8 h, 3 MPa H<sub>2</sub>, and 1.0 g catalyst; (c) effect of H<sub>2</sub> pressure at 200 °C, 8 h, and 1.0 g catalyst; (d) relationship among glycerol conversion, 1,3-propanediol selectivity, and yield compiled from panels (a)–(c).

contrast, product selectivities evolve more rapidly and stabilize earlier, with 1,3-PDO selectivity reaching ~80% by 4–5 h. The selectivities of 1,2-PDO and propanol byproducts decrease correspondingly and remain essentially constant thereafter. The different temporal evolutions of conversion and selectivity indicate that the relative rates of competing hydrogenolysis pathways are established early in the reaction. Once steady selectivity is reached, continued glycerol conversion proceeds without changes in product distribution, suggesting stable active sites and the absence of significant catalyst restructuring or deactivation over the investigated time window. The temperature dependence of catalytic performance, evaluated at a fixed reaction time of 8 h, reveals a pronounced trade-off between glycerol conversion and 1,3-PDO selectivity (figure 4(b)). At low temperatures (160 °C–180 °C), glycerol conversion remains limited (< 5%) despite very high 1,3-PDO selectivity (> 80%–90%), reflecting insufficient thermal activation of C–O bond cleavage. Increasing the temperature to 200 °C significantly enhances conversion while maintaining high 1,3-PDO selectivity (~80%), identifying this condition as a favorable balance between activity and selectivity. Further increases in temperature to 220 and 240 °C result in substantially higher glycerol conversions (exceeding 20% and 30%, respectively), but these gains are accompanied by a sharp decline in 1,3-PDO selectivity and increased formation of 1,2-PDO and propanol products. This behavior indicates the onset of non-selective reaction pathways including over-hydrogenolysis, which become increasingly competitive at elevated temperatures. Hydrogen pressure has a strong influence on glycerol conversion at low pressures but a diminishing effect at higher pressures (figure 4(c)). At 0.1 MPa H<sub>2</sub>, glycerol conversion is negligible (< 0.5%), although 1,3-PDO selectivity exceeds 90%, indicating that hydrogen availability limits the overall reaction rate. Increasing the pressure to 1 MPa modestly improves conversion to ~2%, while further increases to 3 and 5 MPa lead to nearly identical conversions and product

**Table 2.** Catalysts used for figure 5(A) to isolate the effect of Pt site density at nearly constant acidity (Pt/W–KIT-6 series). All site densities are reported as  $\times 10^{-6}$  Kmol kg<sub>cat</sub><sup>-1</sup>.

Catalyst	Dopant	Pt loading (wt%)	Calcination (°C)	Pt sites	Brønsted acid	Lewis acid
C06	W	0.0	550	0.0	0.27	0.06
C11	W	0.2	550	9.7	0.27	0.06
C12	W	0.4	550	19.5	0.27	0.06
C13	W	0.6	550	28.9	0.26	0.06
C14	W	0.8	550	37.7	0.26	0.05
C15	W	1.0	550	45.6	0.26	0.06

**Table 3.** Catalysts used for figure 5(B) to evaluate the effect of Brønsted acid site density at approximately constant Pt site density and low Lewis acidity. All site densities are reported as  $\times 10^{-6}$  kmol kg<sub>cat</sub><sup>-1</sup>.

Catalyst	Dopant	Pt loading (wt%)	Calcination (°C)	Pt sites	Brønsted acid	Lewis acid
C23	W	1.0	650	47.1	0.10	0.05
C22	Nb	1.0	650	47.1	0.12	0.04
C21	Nb	1.0	550	47.6	0.18	0.06
C15	W	1.0	550	45.6	0.26	0.06

**Table 4.** Catalysts used for figure 5(C) to probe the influence of Lewis acid sites using Brønsted-free supports. All site densities are reported as  $\times 10^{-6}$  Kmol Kg<sub>cat</sub><sup>-1</sup>.

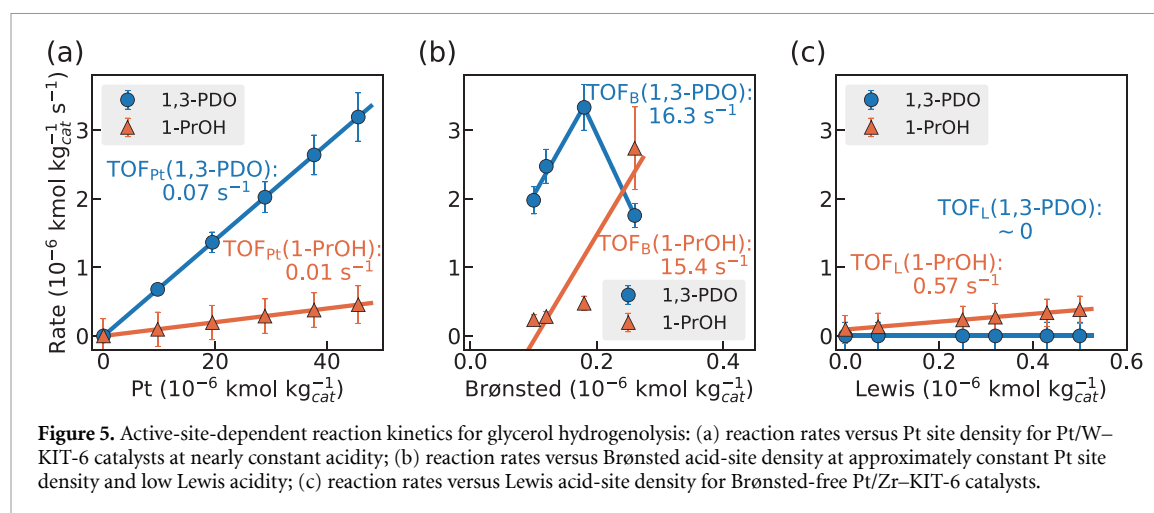
Catalyst	Dopant	Pt loading (wt%)	Calcination (°C)	Pt sites	Brønsted acid	Lewis acid
C20	Si	1.0	550	47.8	0.00	0.00
C24	Zr	1.0	900	46.9	0.00	0.07
C19	Zr	1.0	750	46.9	0.00	0.25
C18	Zr	1.0	650	47.0	0.00	0.32
C17	Zr	1.0	600	47.2	0.00	0.43
C16	Zr	1.0	550	47.7	0.00	0.50

distributions. The insensitivity of catalytic performance above approximately 3 MPa H<sub>2</sub> suggests that hydrogen coverage on the active metal sites becomes saturated and that the reaction rate is no longer limited by hydrogen activation or supply. These results confirm that the standard operating pressure of 3 MPa is sufficient to probe intrinsic catalytic behavior. By compiling data from all experimental conditions, figure 4(d) provides a unified view of the relationship between glycerol conversion, 1,3-PDO selectivity, and yield. At low conversions, 1,3-PDO selectivity increases with conversion, reflecting the dominance of selective C–O hydrogenolysis pathways. At intermediate conversions (approximately 10%–15%), 1,3-PDO selectivity reaches a plateau near ~80%, corresponding to the regime in which selective hydrogenolysis is maximized. At higher conversions (> 20%), 1,3-PDO selectivity decreases sharply, indicating a transition toward unselective reaction pathways. As a consequence, the calculated 1,3-PDO yield exhibits a clear maximum at intermediate conversions, defining an optimal operating window in which conversion and selectivity are favorably balanced. Figure 4 therefore establishes that selective glycerol hydrogenolysis over the C11 catalyst is favored under moderate reaction severity, characterized by intermediate temperatures, sufficient hydrogen pressure, and controlled conversion levels. These results define the catalytic performance baseline for subsequent mechanistic and kinetic analyses and provide guidance for identifying operating conditions that maximize 1,3-PDO yield while suppressing undesired side reactions.

### 3.4. Determination of active sites and their kinetic roles

To enable active-site-resolved kinetic analysis, three systematically designed catalyst sets were employed, as summarized in tables 2–4. These sets independently vary Pt site density (for figure 5(A)), Brønsted acid site density at nearly constant Pt loading (for figure 5(B)), and Lewis acid site density on Brønsted-free supports (for figure 5 C), providing a controlled framework for isolating the roles of individual catalytic functionalities.

The reaction network shown in figure 1 represents lumped reaction pathways constructed from experimentally observable product distributions and established mechanistic sequences reported for glycerol hydrogenolysis over bifunctional metal–acid catalysts. Because short-lived intermediates (e.g. enols, aldehydes, and dehydrated species) cannot be directly quantified under the present reaction conditions,



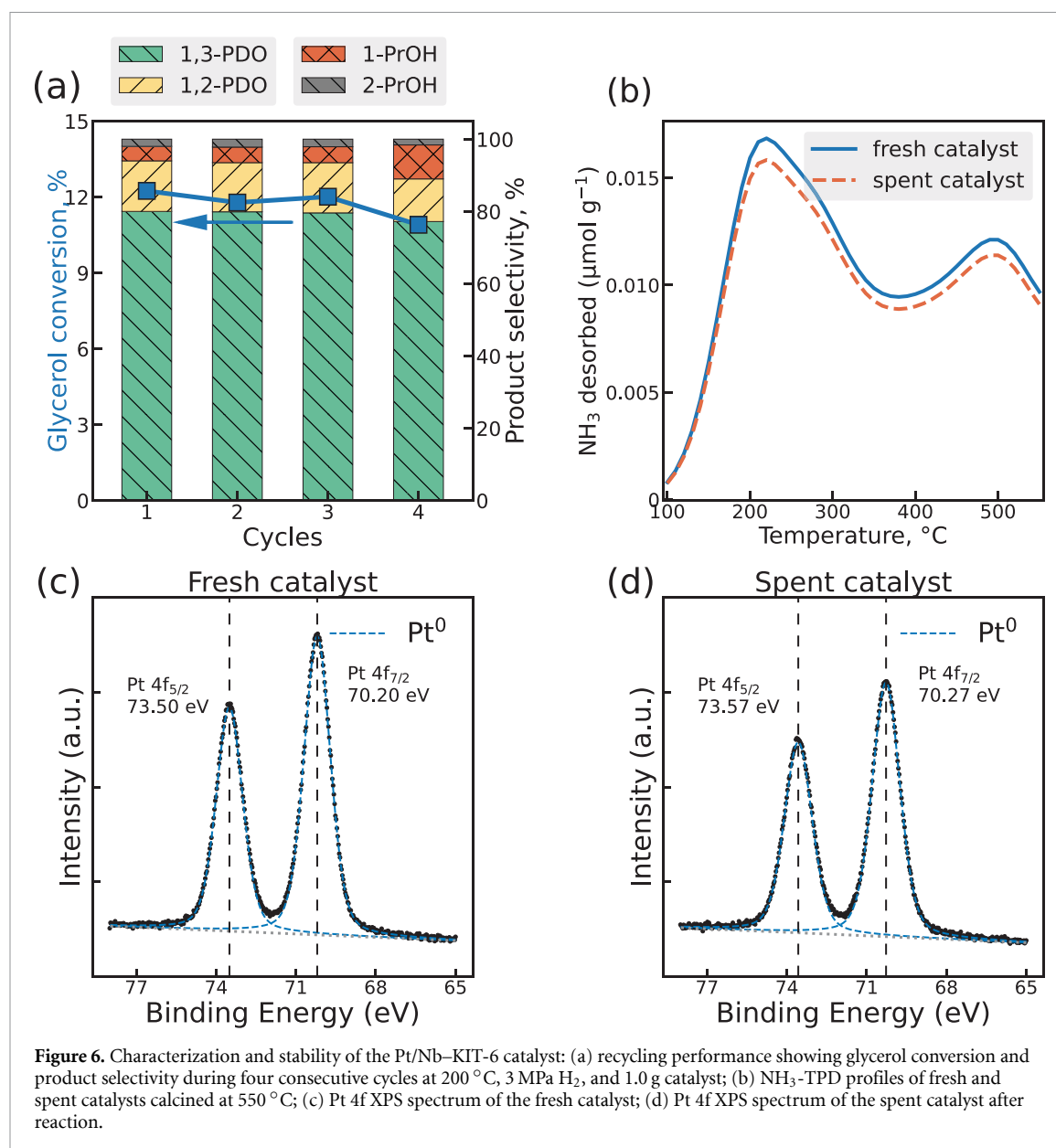
the kinetic analysis focuses on net observable transformations between glycerol and stable products. Consequently, sequential dehydration and hydrogenation steps that occur in rapid succession and cannot be experimentally resolved are grouped into composite pathways (e.g. R1+R2 or R1+R3+R4). The assignment of products to these pathways is based on stoichiometric consistency, literature-reported mechanisms, and the systematic variation of Brønsted and Lewis acidity used in this study to differentiate reaction routes. Figure 5 systematically elucidates the individual and cooperative roles of metallic Pt sites, Brønsted acid sites, and Lewis acid sites in governing glycerol hydrogenolysis kinetics through an active-site-decoupled catalyst design. By leveraging catalyst series in which one class of active sites is varied while the others are held approximately constant, the intrinsic kinetic contributions of each site type can be distinguished without ambiguity from correlated structural or textural effects. Figure 5(a) presents the dependence of reaction rates for glycerol conversion to 1,3-propanediol (R1+R2) and 1-propanol (R1+R3+R4) on the number of exposed surface Pt sites, obtained using the Pt/W–KIT-6 loading series. Across this series, Brønsted and Lewis acid site densities remain nearly constant, enabling isolation of the metal-site contribution. The rate of the glycerol-to-1,3-propanediol pathway (R1+R2) increases linearly with Pt site density over the entire range investigated, indicating that hydrogen activation and subsequent hydrogenation steps occurring on Pt govern the overall rate of the selective hydrogenolysis pathway under standard operating conditions. The corresponding Pt-site-normalized turnover frequency for the R1+R2 sequence is approximately constant ( $\sim 0.07 \text{ s}^{-1}$ ), confirming operation in a Pt-limited regime rather than an acid-limited or transport-limited regime. In contrast, the rate of glycerol conversion to 1-propanol via the consecutive pathway (R1+R3+R4) exhibits a weaker dependence on Pt site density in this moderate-acidity regime, with a substantially lower apparent Pt-site turnover frequency. This behavior indicates that, while Pt is required to supply activated hydrogen for both product channels, metal sites alone are insufficient to drive significant flux toward deeper hydrogenolysis products in the absence of strong acid promotion. These observations establish that an adequate population of accessible Pt sites is a prerequisite for both reaction sequences, but that Pt does not determine product selectivity on its own. Figure 5(b) examines the influence of Brønsted acid site density on reaction rates using catalysts with comparable Pt site densities and minimal Lewis acidity. In this series, the rate of the selective glycerol-to-1,3-propanediol pathway (R1+R2) exhibits a non-monotonic dependence on Brønsted acidity: an initial increase with increasing Brønsted site density is followed by a clear maximum at intermediate acidity, beyond which the R1+R2 rate decreases. To emphasize this behavior, the R1+R2 data are represented by two linear segments: an increasing trend connecting low- to moderate-acidity catalysts, and a decreasing trend connecting the moderate- and high-acidity catalysts. This representation highlights the existence of an optimal Brønsted acid density required to maximize selective glycerol-to-1,3-propanediol conversion. At low Brønsted acidity, insufficient acid functionality limits glycerol dehydration and rearrangement steps preceding hydrogenation, resulting in suppressed R1+R2 rates despite abundant Pt sites. At excessive Brønsted acidity, over-dehydration and secondary acid-catalyzed transformations divert reactive intermediates into the consecutive pathway (R1+R3+R4), leading to a decline in the selective R1+R2 flux. In contrast, the rate of 1-propanol formation via R1+R3+R4 increases monotonically with Brønsted acidity, indicating that stronger or more abundant Brønsted acid sites preferentially promote deeper hydrogenolysis.

Figure 5(c) evaluates the influence of Lewis acid sites using Brønsted-free Pt/Zr-KIT-6 catalysts with systematically varied Lewis acidity. Under these conditions, the rate of the selective R1+R2 pathway remains negligible and essentially independent of Lewis acid density, even though Pt site densities are comparable to those of catalysts active for R1+R2 in figures 5(a) and (b). This result demonstrates that Lewis acid sites do not participate in the glycerol-to-1,3-propanediol pathway. In contrast, the rate of 1-propanol formation via R1+R3+R4 increases modestly with Lewis acid density, indicating that Lewis acid sites favor nonselective pathways such as glycerol isomerization, C–C bond cleavage, or alternative dehydration routes that lead to 1-propanol. The absence of R1+R2 activity on Brønsted-free catalysts further confirms that bifunctional cooperation between Pt and Brønsted acid sites is essential for selective hydrogenolysis. The kinetic results indicate that Lewis acid sites do not promote the selective glycerol  $\rightarrow$  1,3-propanediol pathway under the studied conditions. Increasing Lewis acid-site density does not increase the rate of the selective pathway, indicating that Lewis acidity is not kinetically relevant for this reaction channel. However, minor shifts toward competing products are observed, suggesting that Lewis acid sites may influence parallel pathways by modifying glycerol adsorption geometry and stabilizing alternative dehydration intermediates. Figure 5 establishes that selective glycerol hydrogenolysis to 1,3-propanediol requires the simultaneous presence of (i) a sufficient density of metallic Pt sites to supply activated hydrogen, (ii) a moderate density of Brønsted acid sites to promote controlled dehydration and rearrangement steps associated with R1 and R2, and (iii) minimal Lewis acidity to suppress competing, nonselective pathways associated with R3 and R4. The selective formation of 1,3-propanediol is commonly associated with Brønsted-acid-promoted dehydration of the secondary hydroxyl group of glycerol, followed by hydrogenation on adjacent metal sites. Brønsted acid sites can protonate the hydroxyl group and facilitate regioselective dehydration steps that generate intermediates favorable for 1,3-PDO formation. In contrast, Lewis acid sites typically coordinate with oxygen atoms through lone-pair donation, which modifies the adsorption geometry of glycerol and can favor alternative dehydration pathways. Such coordination may stabilize intermediates leading to competing products such as 1,2-propanediol rather than the regioselective pathway required for 1,3-PDO formation, providing a mechanistic explanation for the negligible contribution of Lewis acidity to the selective 1,3-PDO pathway observed in this study. These results provide a quantitative and site-specific foundation for rational catalyst design and directly motivate the turnover frequency analysis presented in the following section.

### 3.5. Catalyst reusability and stability

The reusability of the Pt/Nb-KIT-6 catalyst was evaluated through four consecutive reaction cycles under standard conditions (200 °C, 3 MPa H<sub>2</sub>, 1.0 g catalyst). As shown in figure 6(a), the glycerol conversion remained nearly constant over the four cycles, indicating excellent catalytic stability during repeated operation. At the same time, the product selectivity was largely preserved, with 1,3-propanediol (1,3-PDO) remaining the dominant product throughout the cycles, accompanied by minor amounts of 1,2-propanediol (1,2-PDO), 1-propanol (1-PrOH), and 2-propanol (2-PrOH). The absence of significant changes in conversion and selectivity suggests that the active sites responsible for glycerol hydrogenolysis remain stable during recycling and that no significant deactivation occurs under the reaction conditions. To further examine possible structural or chemical changes after reaction, the fresh and spent catalysts were characterized by NH<sub>3</sub>-TPD and x-ray photoelectron spectroscopy (XPS). As shown in figure 6(b), the NH<sub>3</sub>-TPD profiles of the fresh and spent catalysts are highly similar, with only a slight decrease in the overall desorption intensity for the spent catalyst, indicating that the acidic properties of the Nb-modified KIT-6 support are largely preserved after reaction. The XPS spectra of Pt 4f for the fresh and spent catalysts (figures 6(c) and (d)) exhibit nearly identical binding energies, with Pt 4f<sub>7/2</sub> peaks located at approximately 70.20 and 70.27 eV, respectively, which are characteristic of metallic Pt<sup>0</sup>. These results indicate that Pt remains predominantly in the metallic state after reaction. The somewhat lower spectral intensity observed for the spent catalyst is likely associated with partial surface coverage by adsorbed reaction species or minor catalyst loss during recovery and handling, rather than changes in the Pt chemical state. Overall, the combined catalytic and characterization results confirm the good structural and functional stability of the Pt/Nb-KIT-6 catalyst under the studied reaction conditions.

While the present work provides active-site-resolved kinetic insight into glycerol hydrogenolysis over bifunctional Pt/KIT-6 catalysts, several limitations should be noted. The kinetic analysis is based on lumped reaction pathways derived from observable products rather than a full elementary-step microkinetic model. In addition, intrinsic kinetic parameters were obtained from batch initial-rate measurements, and further validation under continuous-flow conditions would strengthen reactor-scale interpretation. Finally, the mechanistic interpretation relies primarily on kinetic correlations and controlled variation of Brønsted and Lewis acidity rather than direct *in situ* spectroscopic identification of surface intermediates. Nevertheless, these limitations do not alter the central conclusion that the catalytic contributions of Pt



metal sites, Brønsted acid sites, and Lewis acid sites can be quantitatively decoupled under the investigated conditions.

#### 4. Concluding remarks

This work establishes an active-site-resolved kinetic framework for understanding and controlling the selective hydrogenolysis of glycerol over bifunctional Pt/KIT-6 catalysts. By systematically decoupling and quantitatively correlating the densities of surface Pt sites, Brønsted acid sites, and Lewis acid sites with reaction rates and selectivities, we show that glycerol hydrogenolysis proceeds through distinct, site-dependent pathways whose behavior cannot be rationalized using conventional bulk catalyst descriptors alone. The site-resolved approach links the product distributions directly to the reaction network in figure 1 and provides a quantitative basis for distinguishing selective versus consecutive hydrogenolysis routes. Quantitative rate analysis demonstrates that the formation rates of both 1,3-propanediol and 1-propanol increase with the density of exposed Pt sites under conditions of fixed acidity, confirming that metallic Pt sites are required for hydrogen activation and key hydrogenation steps. Acid functionality, however, dictates how carbon flux is partitioned between selective and consecutive pathways. The selective glycerol-to-1,3-propanediol sequence (R1+R2) exhibits a clear maximum at intermediate Brønsted acid densities, indicating an optimal metal-Brønsted acid cooperation that promotes

selective secondary hydroxyl activation while avoiding over-dehydration. Increasing Brønsted acidity beyond this optimum suppresses the R1+R2 flux and strongly promotes the consecutive route to 1-propanol (R1+R3+R4), consistent with acid-driven dehydration–hydrogenation sequences that favor deeper hydrogenolysis. In contrast, Lewis acid sites alone provide negligible activity toward the selective pathway and primarily enhance nonselective routes, reinforcing that Brønsted acidity is the critical acid functionality for 1,3-propanediol selectivity. The Pt/W–KIT-6 catalyst (0.2 wt% Pt) exhibits a Pt site density of  $9.7 \times 10^{-6} \text{ kmol kg}_{\text{cat}}^{-1}$  together with Brønsted and Lewis acid-site densities of 0.27 and  $0.06 \times 10^{-6} \text{ kmol kg}_{\text{cat}}^{-1}$ , respectively. Under standard conditions (200 °C, 3 MPa H<sub>2</sub>), the catalyst achieves approximately 12% glycerol conversion with ~80% selectivity to 1,3-propanediol. The Pt-site-normalized turnover frequency for the selective glycerol-to-1,3-PDO pathway is approximately  $0.07 \text{ s}^{-1}$ , while Lewis acid sites alone contribute negligibly to this pathway, confirming that selective hydrogenolysis requires the cooperative presence of accessible Pt sites and moderate Brønsted acidity. Turnover frequency analysis further confirms that Brønsted acid sites act as true kinetic promoters rather than spectators: under optimized conditions, their promotion efficiencies exceed intrinsic Pt-site activity by more than an order of magnitude, while excessive Brønsted acidity shifts the system toward the consecutive R1+R3+R4 pathway. These findings clarify long-standing ambiguities regarding the respective roles of metal and acid sites in glycerol hydrogenolysis and provide a quantitative explanation for the wide variability in reported selectivities across nominally similar bifunctional catalysts. This study broadly demonstrates the value of active-site-resolved kinetics as a general strategy for disentangling complex metal–acid reaction networks. Rather than relying on catalyst screening or empirical optimization, the approach presented here enables rational design by explicitly linking reaction pathways to quantifiable site populations and their balance. The design principles identified, a sufficient density of accessible Pt sites coupled with moderate Brønsted acidity and minimized Lewis acidity, are readily extendable to other polyol transformations and multifunctional catalytic systems where selectivity emerges from competition between parallel and consecutive pathways.

## Acknowledgments

This work was supported by start-up funds from the College of Engineering and Science at Louisiana Tech University. This material is also based, in part, upon work supported by the U.S. Department of Energy, Office of Science, Office of Workforce Development for Teachers and Scientists, under the Office of Science Graduate Student Research (SCGSR) program. The SCGSR program is administered by the Oak Ridge Institute for Science and Education (ORISE) for the U.S. Department of Energy under Contract No. DE-SC0014664. We acknowledge additional financial support from the Transportation Infrastructure Research Enhancement (TIRE) Grant from the Louisiana Transportation Research Center (LTRC), and the Research Enhancement Awards (REA) from the Louisiana Space Consortium (LaSPACE). This work was also supported in part by the U.S. National Science Foundation under Grant No. OIA-1946231 and by the Louisiana Board of Regents through the Louisiana Materials Design Alliance (LAMDA).

## Data availability statement

All data that support the findings of this study are included within the article (and any supplementary information files).

## Conflict of Interest

The authors declare no competing financial interest.

## Author contributions

Joaquin Herrero  0009-0008-0512-0606

Conceptualization (lead), Data curation (lead), Formal analysis (lead), Investigation (lead), Methodology (lead), Visualization (lead), Writing – original draft (lead)

Tobias K Misicko  0000-0003-1190-1245

Investigation (supporting), Methodology (supporting), Visualization (supporting), Writing – review & editing (supporting)

Vijaya Gopu  0000-0001-5718-4654

Resources (supporting), Supervision (supporting)

Yang Xiao  0000-0003-1705-2213

Conceptualization (supporting), Funding acquisition (supporting), Resources (lead), Supervision (lead), Writing – review & editing (lead)

## References

- [1] Besson M, Gallezot P and Pinel C 2014 Conversion of biomass into chemicals over metal catalysts *Chem. Rev.* **114** 1827–70
- [2] Pagliaro M, Ciriminna R, Kimura H, Rossi M and Della Pina C 2007 From glycerol to value-added products *Angew. Chem., Int. Ed.* **46** 4434–40
- [3] Bhowmik S and Darbha S 2021 Advances in solid catalysts for selective hydrogenolysis of glycerol to 1,3-propanediol *Catal. Rev.* **63** 639–703
- [4] Miao G, Shi L, Zhou Z, Zhu L, Zhang Y, Zhao X, Luo H, Li S, Kong L and Sun Y 2020 Catalyst design for selective hydrodeoxygenation of glycerol to 1,3-propanediol *ACS Catal.* **10** 15217–26
- [5] Samudrala S P, Kandasamy S and Bhattacharya S 2018 Turning biodiesel waste glycerol into 1,3-propanediol: catalytic performance of sulphuric acid-activated montmorillonite supported platinum catalysts in glycerol hydrogenolysis *Sci. Rep.* **8** 7484
- [6] Khan M S and Khan M M 2025 Promoting effect of silicotungstic acid on selective hydrogenolysis of glycerol to 1,3-propanediol over bifunctional Pt/STA/ $\beta$ zeolite catalysts *Microporous Mesoporous Mater.* **397** 113790
- [7] Greish A A, Finashina E D, Tkachenko O P and Kustov L M 2021 Preparation of propanols by glycerol hydrogenolysis over bifunctional nickel-containing catalysts *Molecules* **26** 1565
- [8] Wang B, Liu F, Guan W, Wang A and Zhang T 2021 Promoting the effect of Au on the selective hydrogenolysis of glycerol to 1,3-propanediol over the Pt/ $\text{WO}_x/\text{Al}_2\text{O}_3$  catalyst *ACS Sustain. Chem. Eng.* **9** 5705–15
- [9] Gallego-García A J 2025 One-pot synthesized niobium-doped nickel catalysts for efficient hydrogen-free glycerol hydrogenolysis *Chem. Eng. J.* **508** 160860
- [10] Mendonca V G S, Freitas I C, Manfro R L and Souza M M V M 2022 Effect of MgO addition to Cu-Ni/ $\text{Al}_2\text{O}_3$  catalysts on glycerol hydrogenolysis in continuous reactor without external hydrogen *Appl. Catal. A* **645** 118838
- [11] Pires M H, Passos F B and Xing Y 2023 Hydrogenolysis of glycerol over ZSM-5 supported ruthenium and copper catalysts: structural study and effects in reaction *Catal. Today* **419** 114161
- [12] Zeng Y et al 2022 Effect of titania polymorphs on the structure and catalytic performance of the Pt- $\text{WO}_x/\text{TiO}_2$  catalyst in glycerol hydrogenolysis to 1,3-propanediol *ACS Sustain. Chem. Eng.* **10** 9532–45
- [13] Salsabila R, Hafidz M, Pratama A A, Sudiyani Y, Marbelia L and Sudibyo H 2025 Design of bifunctional catalyst and kinetic analysis for glycerol conversion to propylene glycol via coupled aqueous-phase reforming and hydrogenolysis *Ind. Eng. Chem. Res.* **64** 23936–51
- [14] Eqi M, Yang Y, Wu G, Li L and Chai Y 2025 Oxygen vacancy engineering on Pt/ $\text{WO}_x/\text{Nb}_2\text{O}_5$  catalysts toward efficient 1,3-propanediol production from glycerol hydrogenolysis *ACS Catal.* **15** 5142–54
- [15] Reynoso A J 2025 Sustainable  $\text{H}_2$ -free glycerol hydrogenolysis to 1,2-propylene glycol using vanadium- and boron-doped nickel catalysts *Appl. Catal. B* **379** 125706
- [16] Zhao B, Zou J, Yao B, Wade A, Liu L, Dong J and He Q 2025 Fabricating hydrogen-rich microenvironment through dual-site catalysts for boosting glycerol selective hydrogenolysis *Appl. Catal. B* **377** 125464
- [17] Deng C, Duan X, Zhou J, Zhou X, Yuan W and Scott S L 2015 Ir-Re alloy as a highly active catalyst for the hydrogenolysis of glycerol to 1,3-propanediol *Catal. Sci. Technol.* **5** 1540–7
- [18] Huang L, Zhu Y, Zheng H, Ding G and Li Y 2009 Direct conversion of glycerol into 1, 3-propanediol over Cu- $\text{H}_4\text{SiW}_{12}\text{O}_{40}/\text{SiO}_2$  vapor phase *Catal. Lett.* **131** 312–20
- [19] Oh J, Dash S and Lee H 2011 Selective conversion of glycerol to 1, 3-propanediol using Pt-sulfated zirconia *Green Chem.* **13** 2004–7
- [20] Tomishige K, Nakagawa Y and Tamura M 2017 Selective hydrogenolysis and hydrogenation using metal catalysts directly modified with metal oxide species *Green Chem.* **19** 2876–924
- [21] Amada Y, Shinmi Y, Koso S, Kubota T, Nakagawa Y and Tomishige K 2011 Reaction mechanism of the glycerol hydrogenolysis to 1, 3-propanediol over Ir- $\text{ReO}_x/\text{SiO}_2$  catalyst *Appl. Catal. B* **105** 117–127
- [22] Zhu S, Qiu Y, Zhu Y, Hao S, Zheng H and Li Y 2013 Hydrogenolysis of glycerol to 1, 3-propanediol over bifunctional catalysts containing Pt and heteropolyacids *Catal. Today* **212** 120–6
- [23] Xiao Y and Varma A 2016 Conversion of glycerol to hydrocarbon fuels via bifunctional catalysts *ACS Energy Lett.* **1** 963–8
- [24] Xiao Y, Greeley J, Varma A, Zhao Z J and Xiao G 2017 An experimental and theoretical study of glycerol oxidation to 1,3-dihydroxyacetone over bimetallic Pt-Bi catalysts *AIChE J.* **63** 705–15
- [25] Xiao Y and Varma A 2017 Kinetics of glycerol conversion to hydrocarbon fuels over Pd/H-ZSM-5 catalyst *AIChE J.* **63** 5445–51
- [26] Wang Y, Xiao Y and Xiao G 2019 Sustainable value-added  $\text{C}_3$  chemicals from glycerol transformations: a mini review for heterogeneous catalytic processes *Chin. J. Chem. Eng.* **27** 1536–42
- [27] Xiao Y, Ramanathan A, Subramaniam B and Varma A 2022 Guaiacol hydrodeoxygenation and hydrogenation over bimetallic Pt-M (Nb, W, Zr)/KIT-6 catalysts with tunable acidity *ACS Sustain. Chem. Eng.* **10** 4831–8
- [28] Weisz P and Prater C 1954 Interpretation of measurements in experimental catalysis *Adv. Catal.* **6** 143–96
- [29] Mears D E 1971 Diagnostic criteria for heat transport limitations in fixed bed reactors *J. Catal.* **20** 127–31